Fission barriers, coupled-channel, and shell effects at the Coulomb barrier in the $A \sim 190$ mass region

B. Djerroud,[1] B. Schaly,[1] S. Flibotte,[1] G. C. Ball,[2] S. Courtin,[3] M. Cromaz,[4] D. S. Haslip,[1] T. Lampman,[1] A. O. Macchiavelli,[4] J. M. Nieminen,[1] C. E. Svensson,[1] J. C. Waddington,[1] D. Ward,[4] and J. N. Wilson[5]

[1]*Department of Physics and Astronomy, McMaster University, Hamilton, Ontario, Canada L8S 4M1*

[2]*TRIUMF, 400 Westbrook Mall, Vancouver, British Columbia, Canada V6T 2A3*

[3]*Institut de Recherches Subatomiques, F-67037 Strasbourg Cedex 2, France*

[4]*Nuclear Science Division, Lawrence Berkeley Laboratory, Berkeley, California 94720*

[5]*Department of Chemistry, Washington University, Saint Louis, Missouri 63130*

(Received 26 August 1999; published 13 January 2000)

A study of the role of coupled-channel effects in the enhancement of the population of high-spin states was undertaken with the reactions ^{48}Ca+^{142}Nd and ^{80}Se+^{110}Pd, near the Coulomb barrier, leading to the same compound nucleus, ^{190}Hg, at the same excitation energy. Statistical calculations with standard values for the level density parameters and fission barriers predict an enhancement of the high-spin population for the more mass-symmetric system, brought about by the coupling to inelastic channels in the fusion process. No enhancement was observed which we interpret as an inadequacy of the fission barriers used, and to the role of the shell corrections, in particular those at the saddle point.

PACS number(s): 25.70.Jj, 24.10.Pa, 24.75.+i

I. INTRODUCTION

Appreciable effort has recently been devoted to study of the entrance channel effects, in particular in the $A \sim 150$ mass region [1–4]. It was found that the population of superdeformed states is enhanced for mass-symmetric reactions relative to mass-asymmetric reactions leading to the same compound nucleus formed at the same excitation energy. This effect was interpreted as being due to the longer fusion time associated with the symmetric partners which allows to neutron emission to compete favorably with fission [1], resulting in an increase of the angular momentum of evaporations residues. However, dissipative collision calculations [5,6] did not support this interpretation. Moreover, a recent study [3] showed that, for a mass-symmetric reaction relative to an asymmetric reaction, there was a large increase in the superdeformed band population and in the superdeformed continuum that could not be explained by time independent statistical model calculations. A dynamical delay in the fission process was introduced [4] to reconcile the experimental observations with statistical model predictions. An earlier study [7] in the $A \sim 130$ mass region, where the fission contribution is negligible, showed that the entrance channel effects are associated with differences in the compound-nucleus spin distributions brought about by coupling to inelastic channels in the fusion process. This effect can be interpreted as due to the fact that, for a given compound nucleus, more symmetric entrance channels are characterized by relatively larger Coulomb repulsive forces, thus a deeper interpenetration is required in order to overcome them and initiate fusion. Consequently, in the fusion of quasisymmetric systems, phenomena such as mutual excitation, shape distortion and nucleon exchanges may occur before the fusion process is started and influence the probability of the system to fuse. [8] The present work reports a study in the $A \sim 190$ mass region near the Coulomb barrier to test our understanding of the coupled-channel effects in a mass region where the fission process is important.

For this particular study, the selected reactions were ^{48}Ca+^{142}Nd and ^{80}Se+^{110}Pd, at bombarding energies of 185 MeV and 304 MeV, leading to the same compound system ^{190}Hg, at an excitation energy of $E^* = 37.1$ MeV and 37.7 MeV, for reactions occurring at midtarget, respectively. These reactions populated mostly the residual nucleus ^{188}Hg through the $2n$ exit channel. The ^{48}Ca and ^{80}Se beams were provided by the 88-Inch Cyclotron at the Ernest O. Lawrence Berkeley National Laboratory. The ^{142}Nd and ^{110}Pd targets consisted of a thin foil of 500 μg/cm^2. Gamma rays emitted by the deexciting nuclei were detected with the 8π Spectrometer [9] which comprises 20 Compton-suppressed HPGe detectors and a 71-element bismuth germanate (BGO) ball used as a γ-ray calorimeter and multiplicity detector. The 8π Spectrometer measures simultaneously the population intensity of discrete states and the γ-ray multiplicity. To the extent that the reactions studied populate the same compound nucleus with nearly the same excitation energy and spin distribution, as shown below by the uncoupled calculation predictions, the differences between the population intensities of a discrete state at a given spin or more simply the difference between the γ-ray multiplicity distributions should be directly related to coupled-channel effects. This technique does not require converting measured γ-ray multiplicities into spin distributions. It has been successfully [7] applied to measure a strong enhancement of the population intensity of the superdeformed band in ^{135}Nd in the ^{74}Ge+^{64}Ni reaction compared with the ^{26}Mg+^{112}Cd reaction. It was shown that the observed differences resulted from a modification of the compound-nucleus angular momentum distribution due to the presence of low-lying vibrational states in the projectile and target nuclei.

II. STATISTICAL CALCULATIONS

In the present work, calculations using the code CCFUS [10] were carried out to estimate the coupled-channel effect

TABLE I. Energies and deformation parameters for the first 2^+ and 3^- excited states.

Nucleus	β_2 : Energy (MeV)	β_3 : Energy (MeV)
^{48}Ca	0.10 : 3.83	0.17 : 4.51
^{80}Se	0.24 : 0.67	0.13 : 2.72
^{110}Pd	0.25 : 0.37	0.14 : 2.04
^{142}Nd	0.10 : 1.57	0.10 : 2.08

on the compound nucleus spin distribution. For each system, coupling to the first excited 2^+ quadrupole vibrational state and the first excited 3^- octupole vibrational state was taken into consideration for both the target and projectile nuclei. The published [11] deformation parameters, β_λ, given in Table I were assumed. The derived compound nucleus spin distributions were then used as input to the Monte Carlo evaporation code EVAPOR [12] in order to calculate the residue entry-spin distributions (i.e., the spin of the state emitting the first γ-ray immediately following the last particle evaporation for nuclei surviving fission). The level density formalism of Gilbert and Cameron [13] and a level density parameter of $a=A/8.0$ MeV^{-1} were assumed. The ratio of the single particle level density of the fissioning nucleus at the saddle point deformation to that of the residual nucleus at the equilibrium deformation following neutron emission, a_f/a_n, was set to unity as suggested in literature [23,24,28]. The code uses the spin-dependent fission barrier derived from the parametrization of Sierk [14]. It has several refinements relative to the rotating-liquid-drop model, such as finite-range effects, discussed in the next section.

The results of the calculations are shown in Fig. 1. The upper panel shows the cross sections when no couplings to low-lying vibrational states are included in the calculations, illustrating the closely matched spin distributions. The middle panel gives the cross sections when coupled channels are taken into account, showing an increase in spin for the ^{80}Se-induced reaction. The lower panel shows, as expected, that in contrast with studies [7] in the $A\sim130$ mass region, much of the extra spin is lost to fission, that originates predominately from high angular momentum states. However a 10 $\hbar$ increase in spin for the ^{80}Se-induced reaction is predicted and this should easily be measurable with the techniques described above.

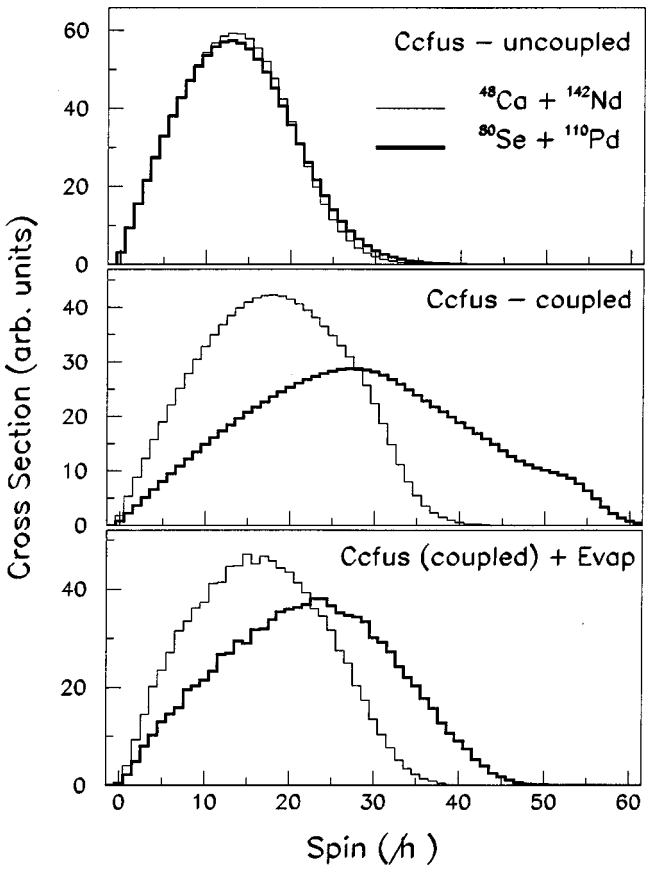

FIG. 1. Calculated compound-nucleus and entry-spin distributions. Upper panel: spin distributions when no coupling to low-lying vibrational states is included in the calculations. Middle panel: spin distributions when coupling to inelastic channels are considered. Bottom panel: entry-spin distributions following the emission of particles for all events surviving fission. Target thicknesses were taken into account by integrating over the appropriate energy spreads. For each panel, the curves were normalized to an equal area.

III. EXPERIMENTAL RESULTS

Shown in Fig. 2 are the measured γ-ray fold distributions for the $2n$ evaporation channel, leading to the residual nucleus ^{188}Hg which represents over 90% of the total fusion-evaporation cross section. The γ-ray fold distributions are directly related to the entry-spin distributions. No centroid shift between the two reactions is seen in contrast with studies [7,15,5] in the $A\sim150$ mass region. Similarly, the intensity profiles as a function of spin of discrete rotational bands are similar for both reactions [16]. One concludes that the entry-spin distributions are identical for the two reactions, in contrast with the theoretical expectations. The γ rays corresponding to the low-lying transitions in ^{80}Se and ^{110}Pd were observed in the present work [16], providing an unambiguous signature of the coupling.

The calculations combining coupled-channel calculations and statistical decay of the compound nucleus described above, were shown [7] to be successful in reproducing the enhancement of superdeformed band population in the $A\sim130$ mass region, where the contribution of the fission process is negligible. In the present work, in the $A\sim190$ mass region, the apparent absence of coupled-channel effects from the entry spin distributions is most likely due to the fission process at high spin which seems to be underestimated in the above predictions. As a first step, the effect of level density on the cooling process was investigated. The level density parameter $a=A/k$ was varied from $k=7$ to $k=11$ within the code EVAPOR, no appreciable differences were observed in the predicted entry-spin distribution relative to those shown and discussed above for $k=8$ in Fig. 1. As a second step, the fission barrier and the ratio of level density parameter (a_f/a_n) were varied. Obviously, a reduction of the fission barrier, or an increase of the a_f/a_n ratio above unity enhances the fission probability. The results are presented in

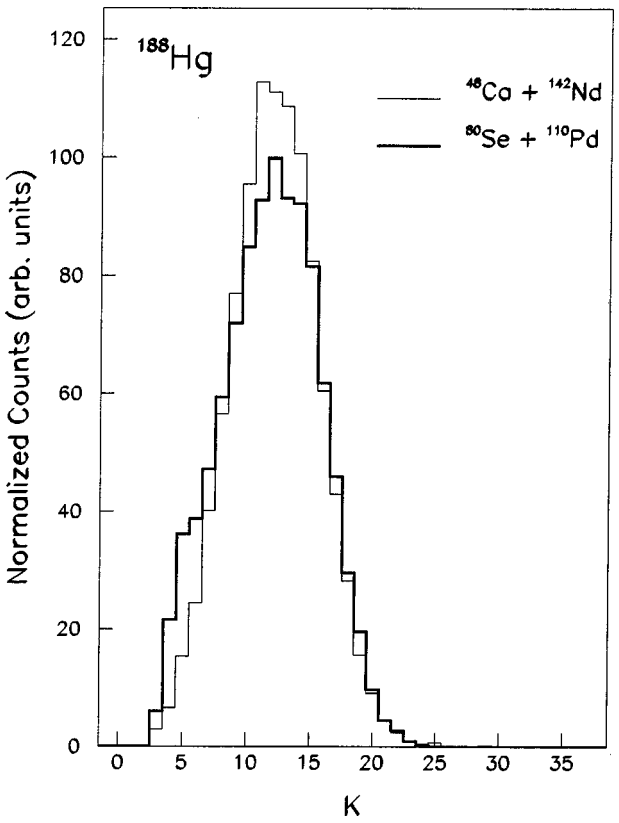

FIG. 2. γ-ray fold distribution, represented by the total number of firing BGO elements, K, measured for the two reactions, for the $2n$ evaporation channel.

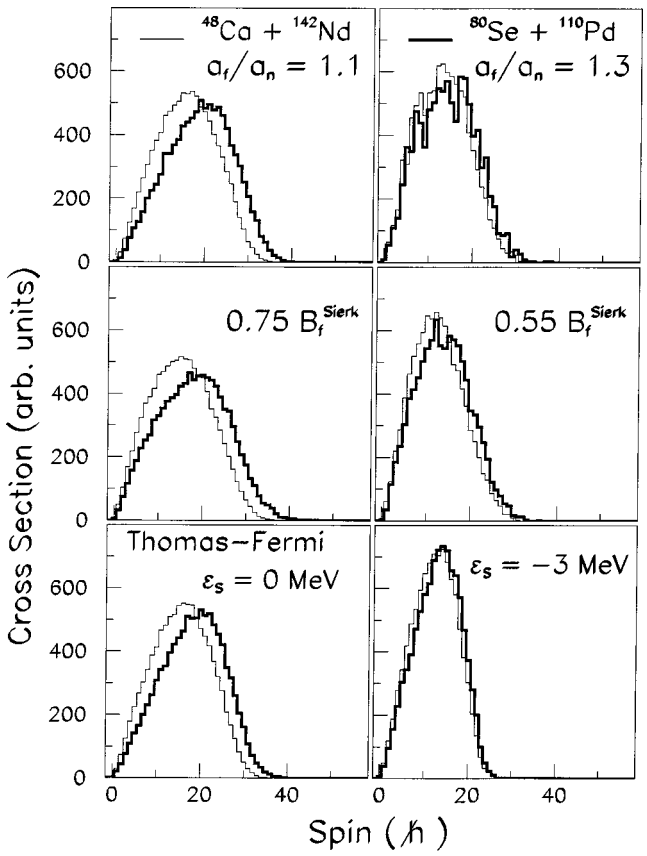

FIG. 3. Comparison of the calculated entry-spin distribution associated with the $2n$ evaporation channel, for the two indicated reactions with the listed values of the statistical model parameters. For the upper panels, the Sierk fission barriers were used and the ratio of level density parameters a_f/a_n was varied as indicated. For the middle panels, the level density parameter a_f/a_n was kept equal to unity and the Sierk fission barriers was multiplied by the indicated factor. For the lower panels, the Thomas-Fermi fission barrier was used without shell correction (left, $\epsilon_S=0$) and with the inclusion (right, $\epsilon_S=-3$ MeV) of shell correction to the barrier (see the text).

the upper and middle panels of Fig. 3. The entry-spin distributions for the $2n$ channel were simulated while increasing the a_f/a_n ratio or reducing the fission barrier, by a scaling factor independent of spin. The parameters were varied until the entry-spin distributions became similar for both reactions as it is observed experimentally. Such an agreement is obtained by reducing the fission barrier by a factor of approximately 0.5 or by increasing the level density ratio by 30% above unity. This drastic reduction of the fission barrier or extravagantly high value of a_f/a_n leads to an unrealistic contribution of fission to the total fusion cross section, of the order of $\sim 78-95\%$ without even the inclusion of the coupled channels, while in this mass region and excitation energy range, it is commonly known that the neutron width dominates the total decay width. The sensitivity of the cross sections to these parameters is illustrated in Fig. 4. The relative contribution of fission cross section to the total fusion cross section, as predicted by the statistical code EVAPOR, is plotted as a function of the level density ratio a_f/a_n (upper panel) and as a function of the fission barrier scaling factor (lower panel). In the former case the Sierk fission barriers were used while in the latter case the level density ratio was set to unity and the Sierk fission barriers were scaled by a factor R ($\leqslant 1$). An increase by two order of magnitude of the fission contribution, in absence of coupling and for both systems, is obtained when the level density ratio or fission barriers are adjusted to reproduce the experimental data. When the couplings to the inelastic channels are included, the contribution of fission is higher for the ^{80}Se-induced reaction, since for this system higher angular momenta are populated.

IV. DISCUSSION

At the incident energies considered in the present work, following the coupled-channels approach, the barrier acts as a divider into two groups of reactions, the direct and fusion reactions. The latter group, investigated in the present work, leads to the formation of an equilibrated compound system that decays in several steps by emission of particles, γ radiation, and/or fission. The excitation energy is high enough to ensure the adequacy of a statistical description of the particle-decay process [17]. As for fission, as concluded by Kramers [18], the dynamical evolution of the compound nucleus from the spherical or near-spherical ground-state shape to the saddle-point deformation is a dissipative process which may depart the fission width from the value predicted by the statistical model and thus cannot be treated in a purely

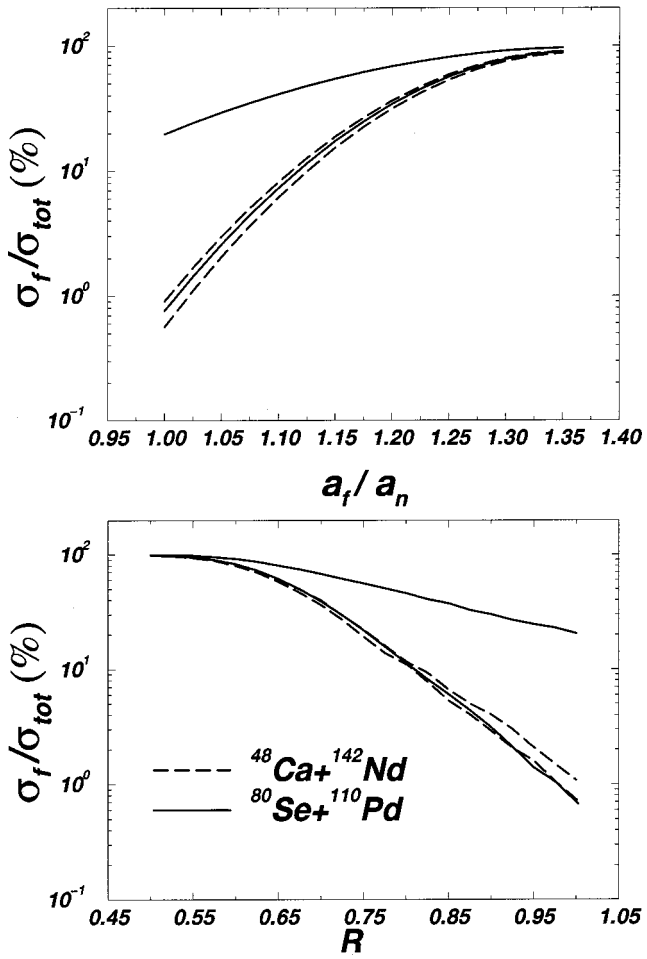

FIG. 4. Dependence of the relative fission cross section on the level density ratio (upper panel) and on the scaling factor for the Sierk fission barrier (lower panel), as predicted by the statistical code EVAPOR. For each reaction, the upper curve represents the calculations when the couplings to the inelastic channels are included.

statistical way, determined by the number of available doorway states above the fission barrier. However, it is experimentally found [19] that the evaporation of particles before scission is enhanced with respect to the statistical model prediction when the excitation energy of the compound nucleus exceeds ~50 MeV. Therefore, this effect will not be considered in the interpretation of the present work, and we will assume that the statistical model is applicable. In fusion-fission studies, the data were usually analyzed following the transition-state statistical model and the rotating liquid drop model (RLDM), the shell effects being neglected at high angular momentum and excitation energy. Fission excitation functions were interpreted within this framework, varying only two parameters: the ratio of the level density parameters a_f/a_n and a scaling factor for the RLDM fission barrier.

A. Level density ratio a_f/a_n

Earlier works on fusion-fission pointed to the fact that a_f/a_n is appreciably larger than unity [20,21], by up to 10 $-20\,\%$, and in order to be consistent with the fact that the shape of the nucleus is changing with angular momentum this ratio would depend on the angular momentum [22]. However, a large correlated range of these parameters, namely the level density ratio and fission barriers, can provide an equally good reproduction of the experimental data. Later studies [23,24] showed that the number of prefission neutrons had a greater sensitivity to the level density ratio than did to the fission barrier, also prescission charged-particle multiplicities placed limits on the level density parameters. The ratio of level densities parameter was found to be consistent with a value of unity. Consequently, the high value of the ratio $a_f/a_n \sim 1.3$ needed to reproduce our experimental data is inadequate.

B. Fission barriers

As for the fission barriers, their prediction relies on the determination of the saddle point in the calculated shape-dependent potential energy surface. The rotating-liquid-drop model [25] has provided a simplified model of the potential energies and equilibrium configurations of rotating nuclei as a function of spin. However, when the liquid-drop model was confronted (within a statistical de-excitation model) with experimental data on heavy-ion-induced fission and evaporation-residue formation, the fission-barrier heights had to be reviewed [14]. A comprehensive survey of macroscopically calculated fission barriers was done by Sierk within the framework of the Yukawa-plus-exponential model [26], leading to a reasonable reproduction of the experimental data on fission and evaporation-residue cross sections [14,24]. This angular-momentum-dependent macroscopic model [14] had several refinements relative to the rotating-liquid-drop model, the most important being the inclusion of finite-range effects in the nuclear surface energy by means of Yukawa-plus-exponential potential, the finite surface diffuseness effects in the Coulomb energy and the rotational moments of inertia. This finite-range rotating liquid-drop model is widely used and included in the current statistical codes [12,27]. In the present work, it was necessary to drastically reduce the Sierk fission barrier, leading to an unrealistic contribution of the fission decay channel to the fusion cross section, as discussed in the previous section. A more recent analysis [28] of ^{3,4}He-induced reactions for a variety of nuclei covering a mass range of $A=186-213$ showed that the fission excitation functions scale according to the transition state model prediction once shell effects are taken into account and that the ratio of level densities parameter (a_f/a_n) was found to be consistent with a value of unity. Bearing in mind the differences observed between fission barriers extracted from the experiments preformed using light projectiles and those using heavy ions [29], where higher angular momenta are involved, an interpretation of the discrepancy observed in this work could be related to the dependence of the fission barrier on the angular momentum. The fission barrier may actually decrease more rapidly with increasing angular momentum when compared to the Sierk fission barrier. Existing microscopic calculations of fission barriers do not provide comprehensive and quantitative predictions, while macro-

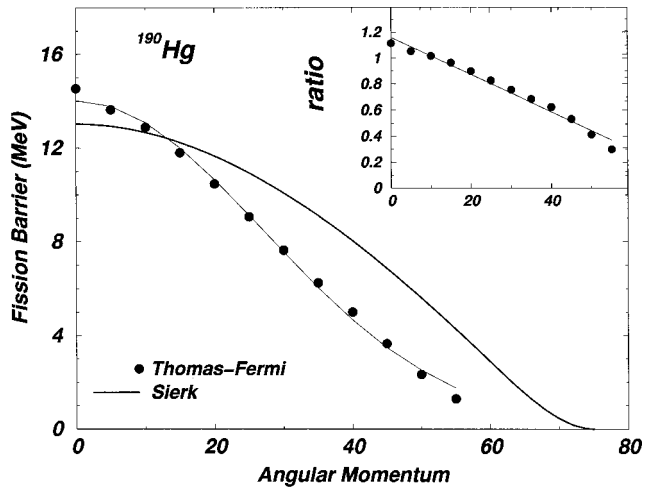

FIG. 5. Dependence of the ^{190}Hg fission barrier on angular momentum as calculated by the Sierk model (continuous thick curve) and the Thomas-Fermi model (full circles) well fitted by a Gaussian distribution (continuous thin curve). The inset represents the ratio of the two barriers, Thomas-Fermi to Sierk, as a function of spin.

scopic theories are inadequate since they are limited to the use of rigid moments of inertia [32]. Recently, Myers and Swiątecki proposed [32] new fission barriers based on the Thomas-Fermi nuclear model [30–32]. This model aims at a macroscopic description of the binding energy considered as a function of the neutron and proton number and of the nuclear shape that includes angular momentum, through a self-consistent, semiclassical, mean-field solution of the problem of self-bound nucleons. It uses an effective velocity- and density-dependent Yukawa interaction between the nucleons. The Thomas-Fermi fission barrier is deduced by tracing out the deformation energy of a nucleus at a given spin as a function of increasing quadrupole moment and then locating the maximum when it exists. For each value of the quadrupole moment, the Thomas-Fermi Euler-Lagrange equations are solved by iteration under the given constraint on the quadrupole moment, through a three-dimensional grid on the neutron and proton density distribution. As this numerical saddle point search is required for each new fission barrier of interest, the usefulness of the Thomas-Fermi model is restricted as regards the use of derived fission barriers within a statistical code. As an alternative for the present work, the Thomas-Fermi fission barrier was calculated for the compound system ^{190}Hg, for various values of the angular momentum, then its parametrization as a function of spin was implemented in the statistical code. Figure 5 displays the calculated fission barrier for the ^{190}Hg nucleus as a function of the angular momentum according to Sierk model (continuous curve), and to Thomas-Fermi model (full circles), where each point represents a complete numerical saddle point search, described above, obtained for the given spin. While at low spin the barriers are similar within 1 MeV, at high spin where the coupled-channel effects are expected to be present (see Fig. 1), the Thomas-Fermi fission barrier decreases more rapidly relative to the Sierk barrier. The inset of Fig. 5 shows that the ratio of the two fission barriers has a nearly linear dependence as a function of spin.

C. Shell effects

In addition, the fission barrier depends on the shell corrections:

$$B_f(J) = B_f^{ld}(J) + (\delta\epsilon_{\rm sad} - \delta\epsilon_{\rm g.s.})$$

where $B_f^{ld}(J)$ is the spin-dependent fission barrier from a macroscopic model and $\delta\epsilon_{\rm sad}$ *and* $\delta\epsilon_{\rm g.s.}$ are the shell corrections at the saddle point and at the ground state, respectively. While the ground state shell corrections are believed to be known within 1 MeV, one cannot exclude the presence of shell effects at the saddle point as it is usually assumed in the literature [29]. Furthermore, little is known on the dependence on spin of shell effects at the saddle point. As the fission barrier puts constraints on the difference $\delta\epsilon_{\rm sad} - \delta\epsilon_{\rm g.s.}$, in the following when referring to the shell correction, the difference is intended and simply indicated by ϵ_S. The shell effects, not included in the calculations presented above, could contribute significantly to the lowering of the fission barrier as the inclusion of shell corrections as a function of deformation alters the potential energy surfaces [33,34]. Microscopic calculations [35], using Strutinsky's method, predict that the shell correction should fluctuate and eventually disappear with increasing angular momentum of the nucleus. This is due to the debunching and rebunching of single particle states due to the increasing deformation of the fast rotating nucleus [29].

To implement the Thomas-Fermi fission barrier in the statistical code, it was found that its dependence on spin (J) follows approximately a Gaussian distribution with a maximum at spin zero (see Fig. 5), and can be written as

$$B_f(J) = B_f(0)\exp(-J^2/2\sigma_J^2) + \epsilon_S,$$

where, for the ^{190}Hg nucleus, $B_f(0) = 14$ MeV and $\sigma_J = 27\hbar$ as obtained from a fit of the Thomas-Fermi fission barrier. The parameter ϵ_S was added to represent the shell correction as the shell effects are disregarded in the Thomas-Fermi fission barrier calculations [32]. The bottom panels of Fig. 3 show the entry-spin distributions for the $2n$ decay channel, calculated with the code EVAPOR, where the Thomas-Fermi fission barrier was used following the parametrization of the fission barrier given above. An agreement with the experimental findings was obtained for shell corrections in the order of $\epsilon_S \sim -3$ MeV. Based on the finite-range droplet macroscopic model and the folded-Yukawa single-particle microscopic model [36] by Möller *et al.*, the ground state shell correction is estimated to be $\delta\epsilon_{\rm g.s.} = -1$ MeV for ^{190}Hg. Thus the inclusion of ground state shell correction alone actually leads to an increase of the fission barrier. While there is the possibility of inaccuracy, the ground-state shell corrections are believed to be known within 1 MeV, thus the total shell correction found above suggests that the shell correction at the saddle point is of the order of $\delta\epsilon_{\rm sad} \sim -4$ MeV. This value, $\epsilon_S \sim -3$ MeV, should be regarded as an approximate average value over spin, of the difference of shell corrections at the saddle point and at the ground state. To illustrate the shell correction order of magnitude, its value for the ground state of various Hg isotopes is displayed

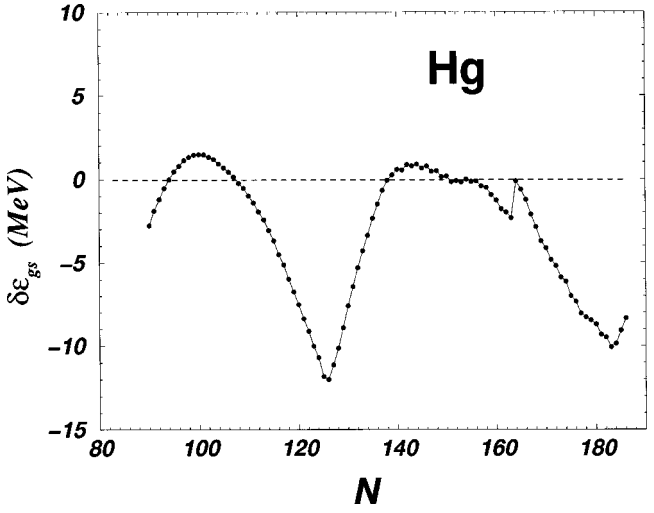

FIG. 6. Calculated ground-state shell correction for the Hg isotopes as a function of the neutron number *N*, based on the finite-range droplet macroscopic model and the folded-Yukawa single-particle microscopic model, from Ref. [36].

in Fig. 6 as a function of the neutron number, as calculated in Ref. [36]. One notices the large minimum at $N=126$, which in absence of shell correction at the saddle point would contribute significantly to an increase of the fission barrier when the neutron number increases, thus an enhancement of shell-stabilization against fission. The contribution of shell effects at the saddle point may however affect this stability. Similarly, in the spherical Th mass region, due to the stabilizing influence of the ground-state shell effects around $N=126$ shell, an enhancement of the cross section of residues, induced by an increase of the fission barriers, was predicted [37]. However, experimentally, a weak enhancement of the survival probability against fission in the deexcitation process was reported [37]. The existence of shell effects at the saddle point may provide an explanation to this apparent damping of shell effects by counteracting the contribution of the ground-state shell correction. More recently, anomalous fission fragment anisotropies were found for $^{12}C+^{198}Pt$ (^{210}Po, $N=126$), and were significantly larger than those predicted by the standard statistical saddle-point model [38]. It was concluded that the shell effects in the potential energy surface is responsible for this behavior. From all the above conclusions, it appears that the inclusion of shell corrections as a function of deformation in a full calculation of potential energy surface, providing a detailed description of the deformation energy landscape in the saddle region, is greatly needed to complement the statistical model calculations.

V. SUMMARY

To summarize, the $^{48}Ca+^{142}Nd$ and $^{80}Se+^{110}Pd$ reactions leading to the same compound nucleus, ^{190}Hg, at the same excitation energy ($E^*\sim 37$ MeV) were studied. In contrast to the $A\sim 130$ mass region the competition between fission and particle evaporation makes difficult the observation of coupled-channel effects in the $A\sim 190$ mass region through γ-ray spectroscopy. According to the predictions of the statistical calculations performed with standard values of level density parameters and fission barrier, an enhancement of high-spin population was expected for the most mass-symmetric system, due to the large contribution of the coupled-channel effects. Surprisingly, this enhancement was not observed. This absence of enhancement is interpreted as being due to the inaccuracy of the fission barrier used. Although the newly proposed Thomas-Fermi fission barrier seems to produce a more realistic dependence on the angular momentum relative to the Sierk barrier, it was shown that, in addition, it is necessary to take into account the contribution from the shell corrections at the ground and at the saddle point. Further detailed potential energy surface up to the saddle region are necessary and would complement significantly the current statistical model calculations.

ACKNOWLEDGMENTS

This work has been funded by the Natural Sciences and Engineering Research Council of Canada (NSERC). We wish to thank R.K. Bhaduri, J.O. Newton, and V.V. Pashkevich for useful suggestions and W.D. Myers and W.J. Świątecki for fruitful discussions and for supplying their code of Ref. [32]. We thank the staff at the 88-Inch Cyclotron Laboratory for providing the beams needed to perform the experiments.

[1] G. Smith *et al.*, Phys. Rev. Lett. **68**, 158 (1992).
[2] S. Flibotte *et al.*, Phys. Rev. C **45**, R889 (1992).
[3] J.M. Nieminen *et al.*, Phys. Rev. C **58**, R1 (1998).
[4] L.H. Zhu *et al.*, Nucl. Phys. **A635**, 325 (1998).
[5] G. Viesti *et al.*, Nucl. Phys. **A579**, 225 (1994).
[6] S. Flibotte *et al.*, Phys. Rev. C **53**, R533 (1996).
[7] J.M. Nieminen *et al.*, Phys. Rev. Lett. **78**, 3832 (1997).
[8] W. Reisdorf *et al.*, Nucl. Phys. **A444**, 154 (1985).
[9] H.R. Andrews *et al.*, ''Proposal for a National Facility - The 8π Spectrometer,'' AECL-8329 (1984); J.P. Martin *et al.*, Nucl. Instrum. Methods Phys. Res. A **257**, 301 (1987).
[10] C.H. Dasso and S. Landowne, Comput. Phys. Commun. **46**, 187 (1987).
[11] P.H. Stelson and L. Grodzins, Nucl. Data, Sect. A **1**, 21 (1965); R.H. Spear, At. Data Nucl. Data Tables **42**, 55 (1989).
[12] Computer code EVAP, by N.G. Nicolis, D.G. Sarantites, and J.R. Beene (unpublished).
[13] A. Gilbert and A.G.W. Cameron, Can. J. Phys. **43**, 1446 (1965).
[14] A.J. Sierk, Phys. Rev. C **33**, 2039 (1986).
[15] J.L. Barreto *et al.*, Phys. Rev. C **48**, 2881 (1993).
[16] B. Schaly, M.Sc. thesis, MacMaster University, 1999.
[17] J.L. Egido and P. Ring, J. Phys. G **19**, 1 (1993).
[18] H.A. Kramers, Physica (Amsterdam) **7**, 284 (1940); P. Grangé, L. Jun-Qing, and H.A. Weidenmuller, Phys. Rev. C **27**, 2063 (1983).

[19] D.J. Hinde, H. Ogata, M. Hanaha, T. Shimoda, N. Takahashi, A. Shinohara, S. Wahamatsu, K. Katori, and H. Okamara, Phys. Rev. C **39**, 2268 (1989).
[20] R.Vandenbosch and J.R. Huizenga, *Nuclear Fission* (Academic Press, New York, 1973).
[21] H. Delagrange, A. Fleury, and J.M. Alexander, Phys. Rev. C **16**, 706 (1977).
[22] M. Beckerman, Phys. Lett. **78B**, 17 (1978).
[23] D. Ward, R.J. Charity, D.J. Hinde, J.R. Leigh, and J.O. Newton, Nucl. Phys. **A403**, 189 (1983).
[24] J.O. Newton, D.J. Hinde, R.J. Charity, J.R. Leigh, J.J.M. Bokhorst, A. Chatterjee, G.S. Foote, and S. Ogaza, Nucl. Phys. **A483**, 126 (1988).
[25] S. Cohen, F. Plasil, and W.J. Świątecki, Ann. Phys. (N.Y.) **82**, 557 (1974).
[26] H.J. Krappe, J.R. Nix, and A.J. Sierk, Phys. Rev. C **20**, 992 (1979).
[27] R.J. Charity *et al.*, Nucl. Phys. **A483**, 371 (1988).
[28] L.G. Moretto, K.X. Jing, R. Gatti, G.J. Wozniak, and R.P. Schmitt, Phys. Rev. Lett. **75**, 4186 (1995); Th. Rubehn, K.X. Jing, L.G. Moretto, L. Phair, K. Tso, and G.J. Wozniak, Phys. Rev. C **54**, 3062 (1996).
[29] A. D'Arrigo, G. Giardina, M. Herman, A.V. Ignatyuk, and A. Taccone, J. Phys. G **20**, 365 (1994).
[30] W.D. Myers and W.J. Świątecki, Nucl. Phys. **A601**, 141 (1996).
[31] W.D. Myers and W.J. Świątecki, Nucl. Phys. **A612**, 249 (1997).
[32] W.D. Myers and W.J. Świątecki, Nucl. Phys. **A641**, 203 (1998).
[33] V.M. Strutinsky, Nucl. Phys. **A122**, 1 (1968).
[34] M. Brack, J. Damgaard, A.S. Jensen, H.C. Pauli, V.M. Strutinsky, and C.Y. Wong, Rev. Mod. Phys. **44**, 320 (1972).
[35] S. Åberg, Nucl. Phys. **A268**, 205 (1990), and reference therein.
[36] P. Möller, J.R. Nix, W.D. Myers, and W.J. Świątecki, At. Data Nucl. Data Tables **59**, 185 (1995).
[37] K.-H. Schmidt and W. Morawek, Rep. Prog. Phys. **54**, 949 (1991).
[38] A. Shrivastava, S. Kailas, A. Chaterjee, A.M. Samant, A. Navin, P. Singh, and B.S. Tomar, Phys. Rev. Lett. **82**, 699 (1999).